Industrial fluxless laser weld-brazing process of steel to aluminium at high brazing speed

Guillaume Filliard [a,b,*], Mohamed El Mansori [a], Lucio Tirado [b], Sabeur Mezghani [a], Christian Bremont [b], Mathieu De Metz-Noblat [b]

[a] Laboratoire MSMP-EA7350, Arts et Métiers ParisTech, Rue Saint Dominique, BP 508, 51006 Châlons-en-Champagne Cedex, France
[b] RENAULT S.A.S., Direction de l'Ingénierie de production Alliance/Direction de l'Ingénierie production véhicule 1, 1 avenue du golf, 78288, Guyancourt, Paris, France

A B S T R A C T

AA6016-T4 aluminium and DX56D + Z140M steel sheets were joined by fluxless laser weld-brazing process in industrial conditions and at high brazing speed reaching 6 m/min with ER4043 $AlSi_5$ filler wire. The configuration studied corresponds to an automotive roof/body-side bond application. For each configuration the energy and feeding rate are computed. The resulted intermetallic layer at the Fe–Al interface and its morphology are investigated through hardness, optical microscopy, EDS and EBSD analysis. The maximum thickness of the intermetallic layer is measured for each configuration. The associated mechanical strength is quantified to evaluate the potential of different configurations for an high brazing speed industrial application. Both, thin and thick intermetallic layer presents specific crystallographic orientation. Thin layer presents a small grains microstructures in the opposite of thick layer with bigger grains. For some samples, specific orientations of the intermetallic needles are observed. The configuration with energy of 600 J/cm and a feeding rate of 1.125 (unit-less) stands out as the most significant with an averaged mechanical strength of 101% of the mechanical properties of the filler wire and intermetallic layer with thickness bellow 2 μm. Mechanical fractures are no longer observed at the Fe–Al interface but occurred in the welded area, between the seam and the aluminium sheet.

Keywords:
Fe–Al dissimilar joints
Flux less laser weld-brazing
Brazing speed
Intermetallic layer
Mechanical strength

1. Introduction

1.1. The joining of steel to aluminium

Since 1970 the legislation for emission of polluting gas was reinforced for most of vehicles. This evolution leads car manufacturers to think about lighter vehicle's design which will consume less fuel. Multi-materials design is largely investigated as a solution to reach that goal. In this purpose, car manufacturers are looking on joining steel and aluminium to replace specific heavy steel parts by aluminium. However, to achieve steel and aluminium joints, that fulfil quality requirements, a suitable joining process has to be used. One of the quality criteria is the mechanical strength of the joints, which has to be sufficient enough to pass the crash tests. Bouché et al. [1] and Yeremenko et al. [2] have pointed out that the mechanical strength of steel and aluminium joint is linked with the formation of Fe- and Al-rich intermetallic layer at the steel–aluminium interface due to the diffusion of iron into molten aluminium. The intermetallic are composed of a main layer and long-shape needles oriented towards the seam [2,3]. The main layer is made up of orthorhombic Fe_2Al_5 phase and needles of monoclinic $FeAl_3$ phase [4–8]. This composition is due to the Gibbs free-energy of the Fe_2Al_5 and $FeAl_3$ phases which are the lowest of the Fe–Al intermetallic family [6]. The hardness of this intermetallic compounds, around 1000 Vickers, can lead to brittle fracture for thick intermetallic layer. Lin et al. [9], among other studies, stated out that the maximum thickness of the intermetallic compounds layer should not be more than 10 μm to avoid brittle breakings at the interface between steel and aluminium. Chacrone [3] and Yeremenko et al. [2] showed that the growth of the reaction layer is led by the temperature and the time of interaction at high temperature, thus by the thermal cycle at the steel/aluminium interface. The welding energy, controlled by the process speed and the heat input, is a critical process parameter

* Corresponding author at: RENAULT S.A.S., Direction de l'Ingénierie de production Alliance/Direction de l'Ingénierie production véhicule 1, 1 avenue du golf, 78288, Guyancourt, Paris, France.
E-mail addresses: guillaume.filliard@renault.com (G. Filliard), Mohamed.ELMANSORI@ensam.eu (M. El Mansori), lucio.tirado@renault.com (L. Tirado), sabeur.MEZGHANI@ensam.eu (S. Mezghani), christian.bremont@renault.com (C. Bremont), mathieu.de-metz-noblat@renault.com (M. De Metz-Noblat).

http://dx.doi.org/10.1016/j.jmapro.2016.12.002

Nomenclature

BCC	Body-centered cubic
BS	Brazing speed (m/min)
CMT	Cold Metal Transfer
E	Energy (J/cm)
FCC	Face-centered cubic
FWS	Filler wire speed (m/min)
GMAW	Gas Metal Arc Welding
P	Power (W)
R	Feeding rate (unit less)
Re, σ	Yield strength (MPa)
Rm	Tensile strength (MPa)
σ_0	Lattice friction stress (MPa)

governing the formation of the intermetallic. In order to achieve joints with sounding properties, process parameters have to be optimised. More precisely, the heat input has to be adjusted to the process speed chosen [7].

The joining of steel and aluminium by weld-brazing process with chemical flux was studied in the last decades with several technologies. During weld-brazing, a filler wire is melted by a heat source to create a seam between the steel and the aluminium parts. While the steel part remains solid, the aluminium is melted with the wire. The chemical flux is used to destroy aluminium oxide which help the creation of the joining by reducing the energy input [7]. However it requires a specific preparation step to apply the chemical product before joining and also cleaning operations after joining. Those constraints are not suitable with an industrial production and can only be conducted during laboratory experimentations.

Weld-brazing of steel to aluminium was achieved with the Cold Metal Transfer (CMT) process and Al–Si filler wire by Cao et al. [10], Lin et al. [9] and Zhang et al. [11] at a brazing speed reaching 1.4 m/min. They demonstrated that joints can be achieved in lap configuration with mechanical strengths between 174 and 200 MPa and limited intermetallic layer around 4 μm. Su et al. [12] and Yagati et al. [13] studied the Gas Metal Arc Welding (GMAW) process in lap configuration with $AlSi_5$ filler wire at a speed of 0.5 m/min and [3.5, 4] m/min respectively. They succeeded to reach a mechanical strength around 200 MPa with a maximum thickness of the intermetallic layer of 4 μm at a brazing speed of 1.4 m/min.

Zhang et al. [14] used the laser key-hole mode in a butt configuration with $AlSi_5$ filler wire to weld-braze steel and aluminium at 1 m/min. They obtained joints with strength of 147 MPa and intermetallic layer around 1.5 μm. Several studies such as Dharmendra et al. [15] and Mathieu et al. [7] interested to the lap configuration with Zn-based filler wire. They obtained mechanical strength between 200 and 220 MPa with a maximal brazing speed of 3.6 m/min. However, Mathieu et al. [7] observed cold cracking of joints and corrosion issue due to the zinc composition of the wire. Mathieu et al. [7] and Vrenken et al. [21] have investigated the laser weld-brazing process with Al–Si filler wire in an angle configuration and a brazing speed between 1 and 3 m/min. They reached mechanical strengths of the joints around 200 MPa with low intermetallic layer thickness less than 5 μm. Seam presents small dilution on the aluminium sheets but large penetration. The uses of flux could be responsible for this morphology, as chemicals of the flux act as tensio-actives elements which change the centrifugal convection, due to the Marangoni effect, to centripetal convection as observed for the steel to steel A-TIG welding process [16].

The weld-brazing process with no uses of flux has been recently investigated by Frank with double beam technology on lap and angle configurations [17]. In this process a pulsed laser beam is superimposed with a continuous laser beam to suppress the oxide aluminium layer replacing in this way the chemical flux. The brazing speed used for experiments is 0.7 m/min, but Frank succeeded to reach the maximal speed of 3.6 m/min. Mechanical strengths of 195.6 MPa, 202.9 MPa and 232.1 MPa were achieved with respectively $AlSi_5$, $AlSi_{12}$ and $ZnAl_2$ filler wire.

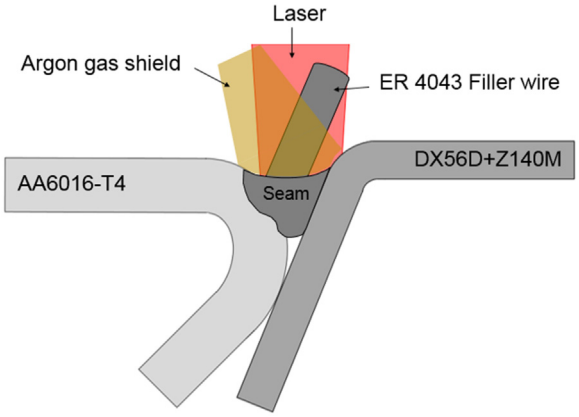

Fig. 1. Schematic section of the industrial aluminium roof/steel body side configuration. The position of the laser, the steel and aluminium sheets, the filler wire and the gas protection are represented.

1.2. Study conditions and procedure

However, if all those studies reveal the potential of joining steel and aluminium they also are limited for an industrial automotive application which has to fulfil the following criteria: flexible positioning of the weld-brazing tool to join long curved parts, high brazing speed (at least 4 m/min) to insure a high industrially production rate and no pre- and post-process operation on the base materials, such as oxide removal by flux and cleaning of seams.

Moreover, Mathieu et al. [7] and Pena [8] demonstrated that the geometry of the seam, which change from lap, angle or butt configuration, and the length of the steel/aluminium interface also influence the mechanical properties of joints. Hence, the type of configuration used when joining steel and aluminium and the influence of the brazing speed on the geometry of the seam are also critical and shall be taken into account.

In this study, the fluxless laser weld-brazing process is studied to join steel and aluminium sheets with Al–Si filler wire at a high brazing speed between 4 and 6 m/min. The configuration studied stems from an angle configuration and corresponds to typical roof/body side joint. The process parameters and their influence on the quality of the joint are analysed. Particularly, the reproducibility of the mechanical properties and the impact of the brazing speed on the intermetallic layer thickness and on the geometry of the seam are investigated. The whole system used for the experiments is fully robotised and similar to the laser installation of an automotive plant.

2. Experimental

2.1. Weld-brazing process

A specific automotive configuration derive from an angle configuration is investigated. It represents the bounding between an aluminium roof and the steel body side of the car. The length of the sheets is 500 mm. A schematic section of the configuration is given in Fig. 1.

Dimensions of both, the aluminium and steel parts, are given in Fig. 2a and b.

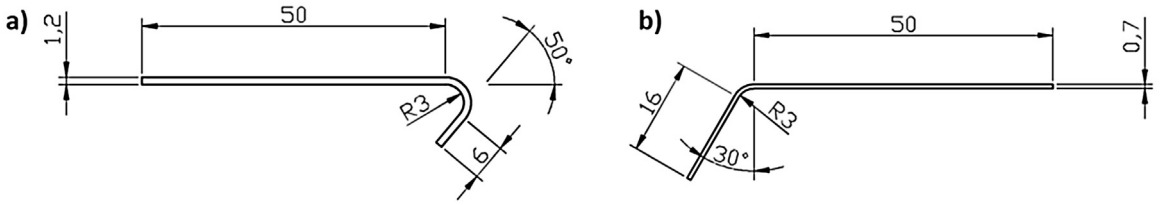

Fig. 2. Dimensions of the aluminium (a) and steel (b) parts.

The laser beam is obtained from a diode source (from Laserline—maximum power 6 kW) perpendicular to the sheets through an optical fibre and a laser head (ALO_3 from Scansonic). The laser head, the optical fibre and power supply cables are fixed on 0 + 6 axis robot (from ABB) which drives the brazing speed. The diameter of the laser spot is 3 mm which is obtained by defocusing the laser from 60 mm above the sheets. The position of the laser with the wire and the laser head is adjusted before weld-brazing with a camera module of the laser head (from Scansonic). The position of the laser can be shift on the one of the base materials. Fig. 3 represents the adjustment of the position of the laser spot with the wire, the laser head and the base materials.

The angle of the filler wire to the sheets is maintained at 15° by a filler wire torch (from Fronuis). Argon with flow rate of 10 L/min was used as shielding gas, feed in the opposite side of the filler wire. The filler wire is pre-heated by a hot wire source (from Fronius) set to 150 A. The sheets are fixed with a holder. A global view of the installation is given in Fig. 4.

The brazing speed is taken between 4 and 6 m/min. A brazing speed of 4 m/min represents the minimal speed to weld-braze 30 roofs in one hour with one laser installation. Two variables are used to assess each experimental test configuration namely the energy and the feeding rate. They are obtained by using the following equations as defined by Koltsov et al. [18]:

$$E = (60 \times P)/(100 \times BS) \quad (1)$$

$$R = FWS/BS \quad (2)$$

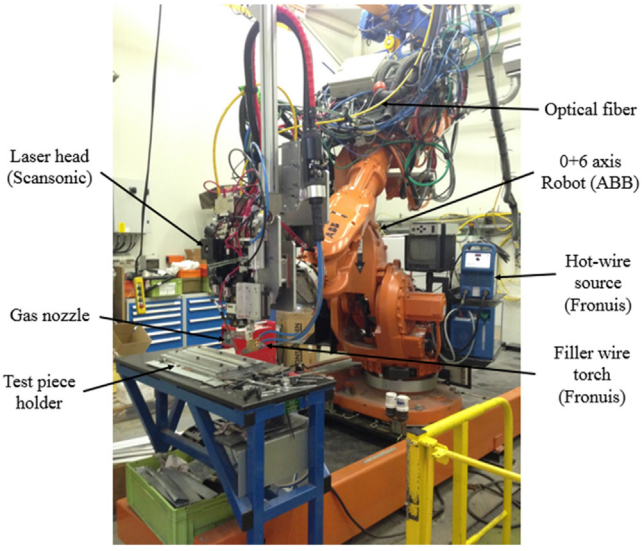

Fig. 4. Laser weld-brazing system for industrial application. Positions of the main components of the installation are given.

With E the energy per unit of length in J/cm, P the power in W, BS the brazing speed in m/min, R the feed rate and FWS the filler wire speed in m/min. The experimental tests setups are listed in Table 1.

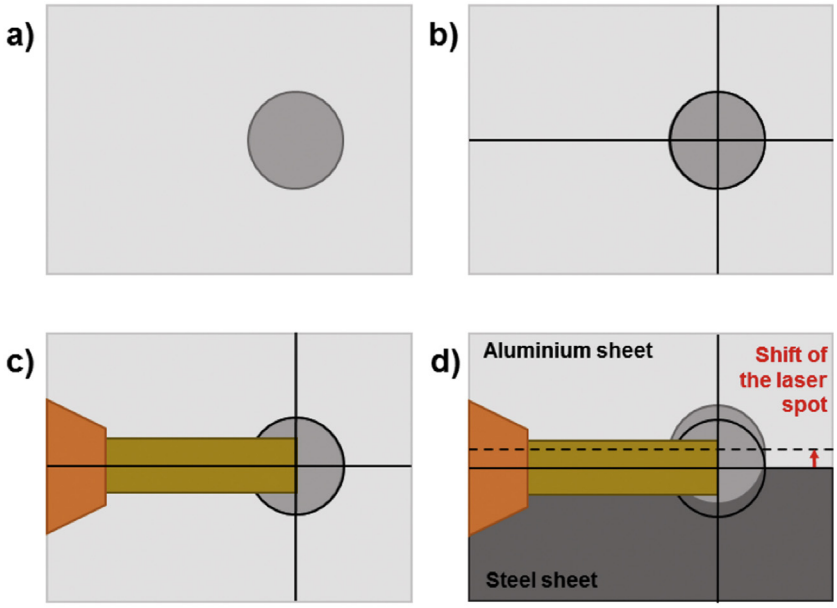

Fig. 3. Adjustment of the position of the laser spot, the wire and the base materials, (a) initial spot laser position, (b) adjustment with the laser head, (c) adjustment with the wire, (d) shift of the laser spot on one of the base materials, here the aluminium plate.

Table 1
Overview of the considered process tests settings.

Configuration number	Energy "E" (J/cm)	Feeding rate "R" (unit less)
1	500	0.917
2	545	1
3	600	1.1
4	600	1.125
5	600	1.222
6	667	1.222
7	750	1.375

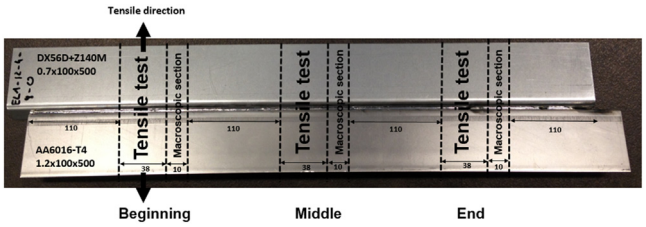

Fig. 5. Positions of the 6 samples for tensile tests and macroscopic section on the test pieces. Each sample is cut for analysis.

2.2. Materials

Sheets of DX56D + Z140M galvanised steel with a thickness of 0.7 mm and AA6016-T4 aluminium with a thickness of 1.2 mm were weld-brazed with an ER4043 $AlSi_5$ filler wire of diameter 1.6 mm. The chemical composition and mechanical properties of base materials and filler wire are given in Table 2.

2.3. Analysis methods

15 weld-brazed test pieces were produced for each configuration tested. Sheets are not cleaned by flux before the weld-brazing process. The mechanical strength of joints is quantified after the weld-brazing operation by a tensile test and the maximum thickness of the intermetallic layer can be measured with an optical microscope. Test pieces were cut in 6 samples, 3 samples for tensile tests ($1 \times 38 \times 100$ mm) and 3 for macroscopic section ($1 \times 10 \times 100$ mm), at the beginning, the middle and the end of the seam (Fig. 5).

Tensile tests were performed with a tensile-testing machine EZ 50 (50 kN, Lloyd Instruments). Macroscopic section are coated with diallylphtalate glass fibre XDPB (NX MET) and phenosplastes resin. The coated samples were pre-polished with abrasive paper (grains of 320, 800 and 1200) and polished with polishing sheets (6, 3 and 1 μm). The polished samples were then observed by optical microscopy with a Nikon Epiphot 200 inverted metallurgical microscope.

Intermetallic layer was also investigated with a Scanning Electron Microscope (SEM). Chemical composition of the layer was obtained through Energy Dispersive Spectroscopy analysis (EDS) and Electron BackScattered Diffraction (EBSD) analysis was carried out to identify the morphology of grain and the crystallographic structure of the intermetallic phases of both a thin and thick intermetallic layer. Both EDS and EBSD analysis were conducted with a constant voltage of 15 keV. The hardness of the main intermetallic layer was measured thanks to a micro hardness tester LEICAVMHT and an iris CCD camera from Sony.

3. Results and discussions

General observations, made during measurements, are given in the first subsection with the analysis of the intermetallic compounds. The second one is focused on the presentation, the analysis and the discussion of the influence of the process parameters on the thickness of the intermetallic layer and the mechanical strength.

3.1. Seam shape and intermetallic layer

Weld-brazed joints present a continuous seam with a smooth surface regardless of the tensile test results and intermetallic measurements (Fig. 6a and b).

Some joints present classical weld-brazing defects such as holes, pinholes, discontinuity, deported seam, weld bead or un-melted wire when the parameters are not well fitted. For a specific feed rate, holes were observed when the energy given to the wire was excessive and un-melted wire was obtained when the energy was insufficient.

In order to analyse the morphology of the intermetallic layer, the brazed interface is divided into three zones 1, 2 and 3, as shown in Fig. 7.

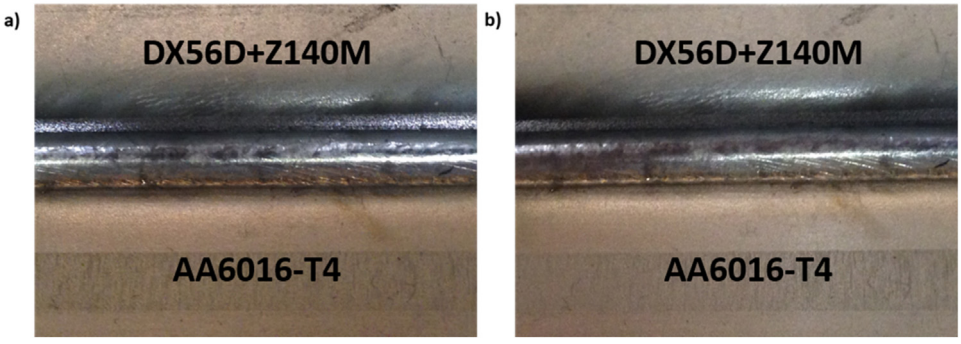

Fig. 6. Examples of the external surface of the seam, they present smooth aspect with few chevron.

Table 2
Chemical compositions and mechanical properties of base metals and filler wire.

Materials	Chemical composition (wt.%)								Mechanical properties	
	C	Si	Mn	Mg	Fe	Zn	Cu	Al	Re (MPa)	Rm (MPa)
DX56D + Z140M	0.002	0.006	0.105	–	Bal.	–	–	–	120–180	260–350
AA6016-T4	–	1.0–1.5	<0,2	0.25–0.6	<0.5	<0.2	<0.2	Bal.	90–120	245
ER4043 ($AlSi_5$)	–	4.5–6.0	0.05	0.05	0.8	0.1	0.3	Bal.	–	120

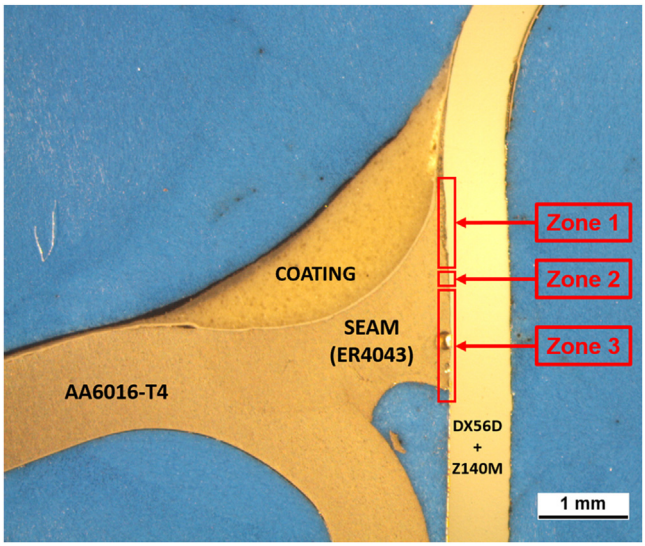

Fig. 7. Optical microscopy observation of cross section of the joint showing the three zones 1, 2 and 3 of the intermetallic layer at the interface between the seam and the steel sheet. Positions of the steel and aluminium sheets and of the seam are presented. A protection coat is applied after the weld-brazing operation above the seam.

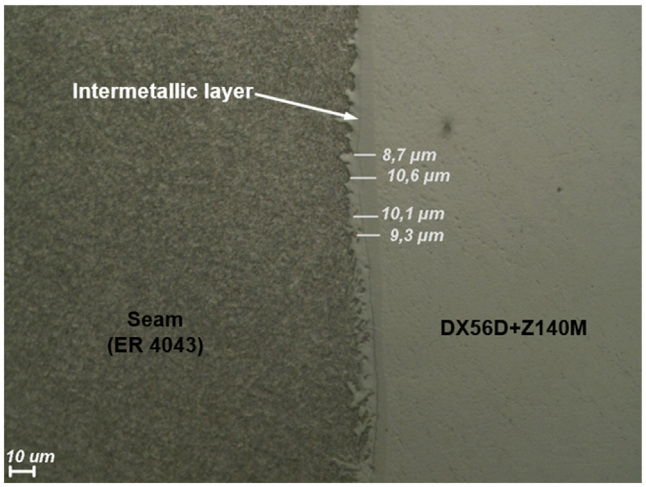

Fig. 8. Measurements of the maximum thickness of the intermetallic layer by optical microscopy.

The intermetallic layer initiates at the top of the seam in zone 1 and its thickness increases until a maximum reached in zone 2. This maximum is followed by a decrease in the thickness of the layer in zone 3 until the layer is no more detectable by optical microscopy. This maximum was measured on each polished samples. An example of the measurement is shown in Fig. 8.

Needles with long shape beginning at the boundary between the intermetallic layer and the seam were observed when the main intermetallic layer is higher than 2–3 µm. Needles globally present an orientation towards the seam in the diffusion direction with a maximum size of 47,3 µm. However, observations also revealed intermetallic needles with specific orientations. A top-down orientation in zone 1 before the maximum thickness and a down-top orientation in zone 2, where the thickness start to decrease, were observed for this samples (Fig. 9).

This specific orientation are attributed to the convection motion in the molten pool which will locally influence the growth of the needles. The modification of the superficial tension with the temperature lead to a Marangoni centrifugal convection flow in the top part of the molten pool and induced centripetal convection in the down part of the molten pool. The “bridge” morphology of the seam is also a consequence of the convection flows. The Marangoni convection attracts the middle of the molten pool towards the surface and generate the convex bottom surface of the seam. Thus this convection flows tend to decrease the middle section of the seam in the opposite of the experiments using chemical flux (Fig. 10).

An averaged hardness of 1063 Vickers was measured for the intermetallic layer. Hardness of the needles could not be measured due to their very limited size. The chemical analysis revealed an intermetallic layer constituted of 66.5% of aluminium and 27.6% of iron and a composition of 74.5% of aluminium and 21.5% of iron

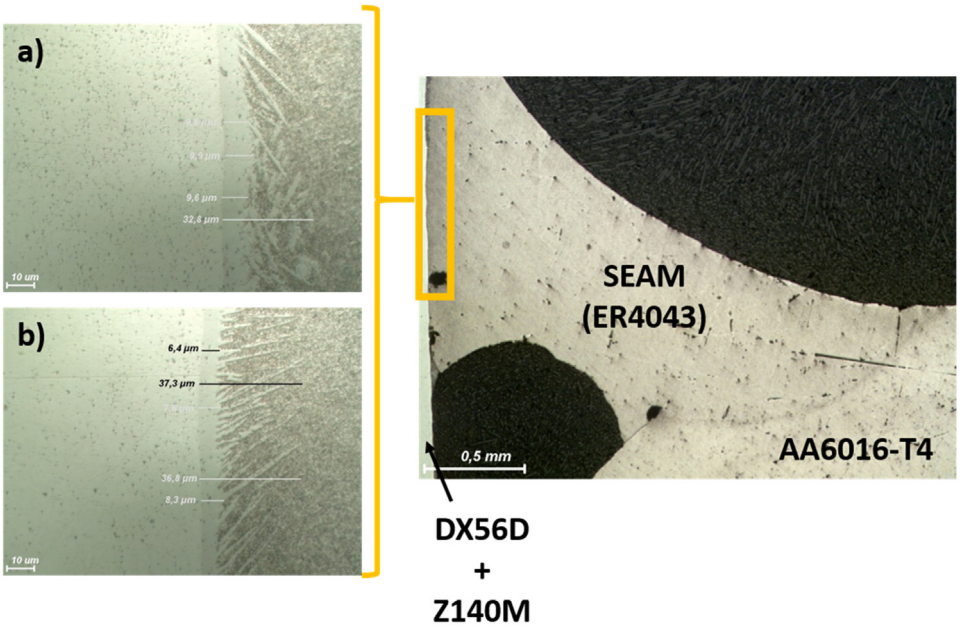

Fig. 9. Orientations of the intermetallic needles observed during optical microscopy, (a) top-down orientation in zone 1 and (b) down-top orientation in zone 2.

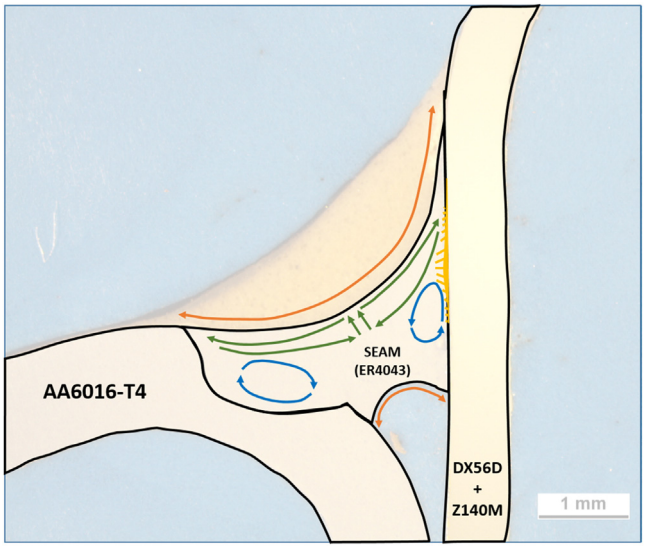

Fig. 10. Convection flows in the molten pool, Marangoni flows in green and induced convection flows in blue, influencing the orientation of the intermetallic needles represented in yellow. The "bridge" morphology of the seam is illustrated by the orange arrows. (For interpretation of the references to colour in this figure legend, the reader is referred to the web version of this article.)

for the needles. Those two elements confirm that the main layer is composed of Fe_2Al_5 and the needles of $FeAl_3$. Thus it can be concluded that there is no different composition of the intermetallic layer at low and high brazing speed.

The EBSD analysis revealed orthorhombic and monoclinic structures for respectively the main layer and the needles. The distribution of the phases, of the all Euler angles and of the main angle deviation obtained for a thin intermetallic layer are displayed in Fig. 11.

Grains of the intermetallic phases are revealed with the all Euler angles map. It can be observed that the layer is constituted of small grains with averaged length of 0.05 μm. EBSD analysis was also done for samples with thick intermetallic layer. The result is given in Fig. 12.

Thicker intermetallic layer revealed to have been constituted of less but bigger grains, than thin intermetallic layer, with averaged grains length of 30 μm. This element showcase that thick intermetallic layer is inclined to diffuse in a privileged way fractures and will lead to ruptures of joints not only because intermetallic compounds have high hardness but also because they are constituted of big grains. For thin intermetallic layer, the mechanical stress is spread on a high number of grains which also will impede the movement of dislocation. This phenomenon also explains the higher mechanical strength of thin intermetallic layer and can be mathematically expressed by the Hall–Petch relationship [19,20]:

$$\sigma = \sigma_0 \times (k/\mathrm{sqrt}(d)) \quad (3)$$

With, σ the yield stress (MPa), σ_0 is the lattice friction stress to move dislocation (constant, MPa), k is the material-dependant Hall–Petch slope (constant, MPa $m^{-1/2}$) and d the average size grain (m) [19,20]. Figs. 11 and 12 also reveal a privileged growth direction of intermetallic grains parallel to the steel/Al interface.

The EBSD analysis also reveal specific crystallographic texturisation of intermetallic grains as it can be seen on the pole figures bellow for thin (Fig. 13) and thick (Fig. 14) intermetallic layer.

Poles figures indicate that both thin and thick intermetallic layer present specific crystallographic texturisation. The crystal orientation for each grain can be observed with the poles figures.

Globally, there is no possibility to distinguish joints with low or high tensile strength and low or high thickness of the intermetallic layer by controlling the external shape of the seam. The quality of the weld-brazed joint can be quantified only by a post process inspection via destructive analysis. Online control processes such as profilometer based on laser triangulation, are not efficient to completely check the quality of steel and aluminium weld-brazed joint. They can only be used after the weld-brazing operation to check the presence of weld-brazed defects in the seam. Thus, in order to ensure the quality during an industrial production, car manufacturers should combine control process to detect weld-brazed defects and periodic destructive tests on samples taken randomly from the production.

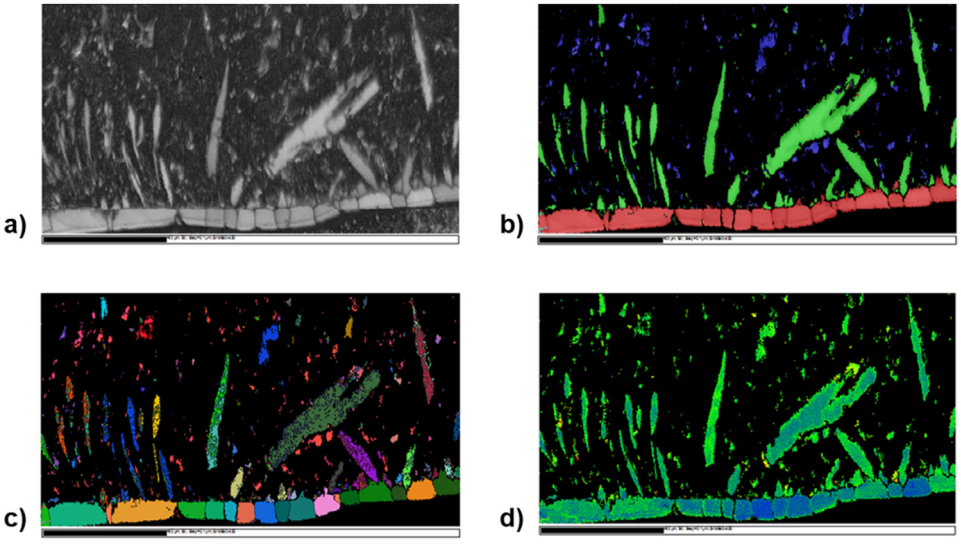

Fig. 11. Results of the EBSD analysis for a thin intermetallic layer. (a) Area investigated, (b) distribution of the different phases, orthorhombic in red, monoclinic in green and cubic in blue corresponding to the *Al99Si* element, (c) all Euler angles and (d) main angle deviation, green and blue correspond to low deviation. (For interpretation of the references to colour in this figure legend, the reader is referred to the web version of this article.)

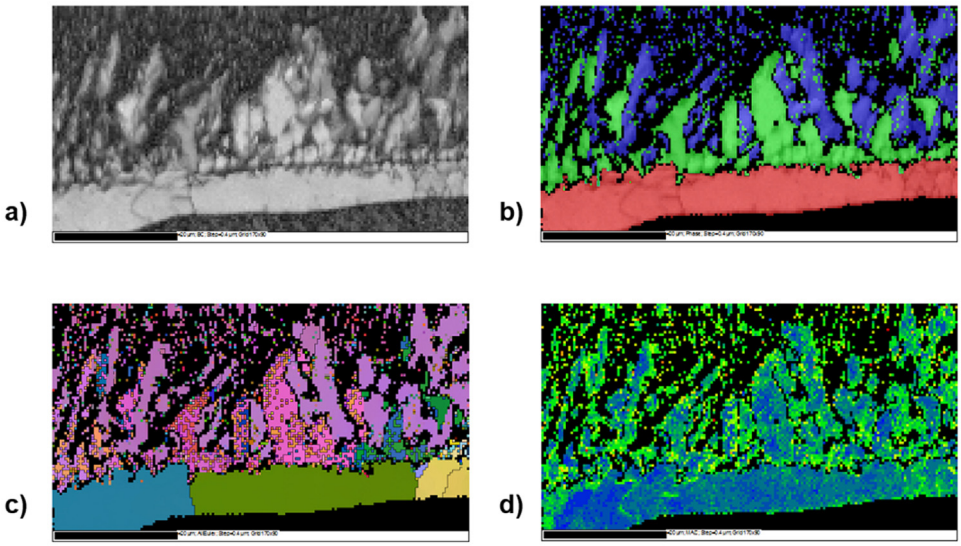

Fig. 12. Results of the EBSD analysis for thick intermetallic layer. (a) Area investigated, (b) distribution of the different phases, orthorhombic in red, monoclinic in green and cubic in blue corresponding to the *Al*99*Si* element, (c) all Euler angles and (d) main angle deviation, green and blue correspond to low deviation. (For interpretation of the references to colour in this figure legend, the reader is referred to the web version of this article.)

3.2. Influence of the process parameters on the intermetallic layer thickness and the mechanical strength

The influence of the process parameters on the intermetallic layer and the mechanical strength has been studied for several combinations of the energy and the feeding rate. The averaged maximum thickness of the intermetallic layer measured is plotted on Fig. 15.

Averaged measurements of the intermetallic layer vary from thicknesses between 2 and 7 μm with low and high dispersion. The thickest intermetallic layer, which also have the highest dispersions, are brought by levels of energy of 600 and 667 J/cm. The impact of the evolution of the feeding rate for the energy level of 600 J/cm on the intermetallic layer is displayed for configurations 3, 4 and 5 in Fig. 9. The thinnest layer is measured for the feeding rate of 1.125, which corresponds to the best compromise between the power given to the materials and the brazing speed used. In the case of configuration 3, it can be assumed that the thick intermetallic layer is a consequence of a too low filler wire speed involving that too much power is given to the steel sheet. Thus the temperature reached at the steel/seam interface is higher than in configuration 4. This difference of temperature explains why the growth of the intermetallic layer is more important for configuration 3 than for configuration 4. Even more, a second phenomenon can be assumed to be responsible for the thickness of the layer of configuration 5. In this case, the brazing speed is lower that for configuration 4. Thus the time of interaction at high temperature, which is directly linked with the growth of the intermetallic layer, increase. In a similar manner it can be observed, for configurations 5 and 6 at a constant feeding rate, a thicker layer when the energy increase. The extra 67 J/cm are partially absorbed by the steel sheet, increasing the temperature reached at the steel/seam interface and generating a thicker intermetallic layer. In order to get the lowest intermetallic layer with low dispersion the right combination has to be founded between the power, the brazing speed and the filler wire speed. Two configurations showed averaged maximal thickness below 2 μm for low energy level of 500 and 600 J/cm and feeding rate of 0.917 and 1.125, they also brought the two lowest dispersions. These results confirm the close dependence of the diffusion mechanism, which controls the growth of the intermetallic layer, to the involved temperature and the time of interaction particularly at high temperature.

The averaged mechanical strength obtained for the 7 configurations is plotted on Fig. 16.

It can be observed that the lowest and highest strengths are measured for the configuration with, respectively, the highest and lowest intermetallic layer, showing the strong dependency of the mechanical strength on the intermetallic layer. This dependency can be more easily observed in Fig. 17.

From our measurements it can be assumed that in our configuration and at our brazing speed, the intermetallic layer should be kept lower than 5 μm rather than 10 μm to insure the highest mechanical strength. A maximum of 121 MPa is reached with energy of 600 J/cm and a feeding rate of 1.125. In this case, ruptures are no more observed in the intermetallic layer and takes place every time in the welded area, between the seam and the aluminium sheet (Fig. 18).

The two lowest averaged mechanical strength of 86 and 84 MPa are measured for the thickest intermetallic layer. The fracture of test specimens during loading manifests itself at the interface between the seam and the steel sheet, where the intermetallic layer is located (Fig. 19).

These results point out that it is possible to find a configuration with a high brazing speed which will generate a thin intermetallic layer and a high mechanical strength. However, they also bring out that the energy level has to be chosen very carefully according to the feeding rate to insure a good equilibrium between the necessary amount of power given to the materials and the brazing speed.

4. Conclusions

Fluxless steel/Aluminium laser weld-brazing experiments at high brazing speed and in industrial context were performed. Results highlight that:

(1) Thin and thick intermetallic layers show specific microstructures and crystallographic orientations with small grains organisation for thin layer and bigger grains for thick layer.

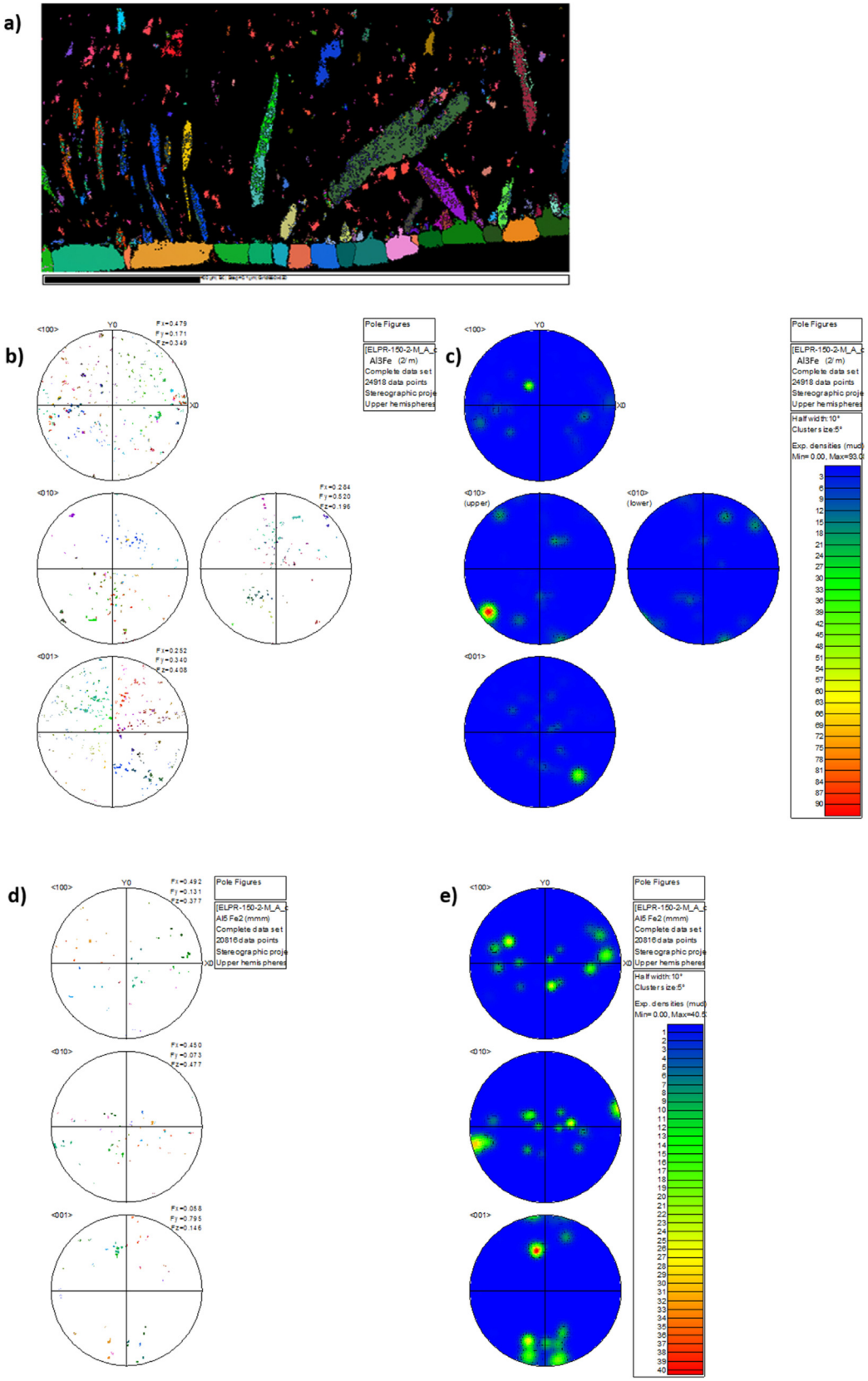

Fig. 13. Crystallographic orientations of grains of a thin intermetallic layer, for the needles (b) and for the main layer (d). Specific orientations of grains could be identified when the density, represented by the coloured scale, respectively for the needles (c) and for the main layer (e), is high (in red). (For interpretation of the references to colour in this figure legend, the reader is referred to the web version of this article.)

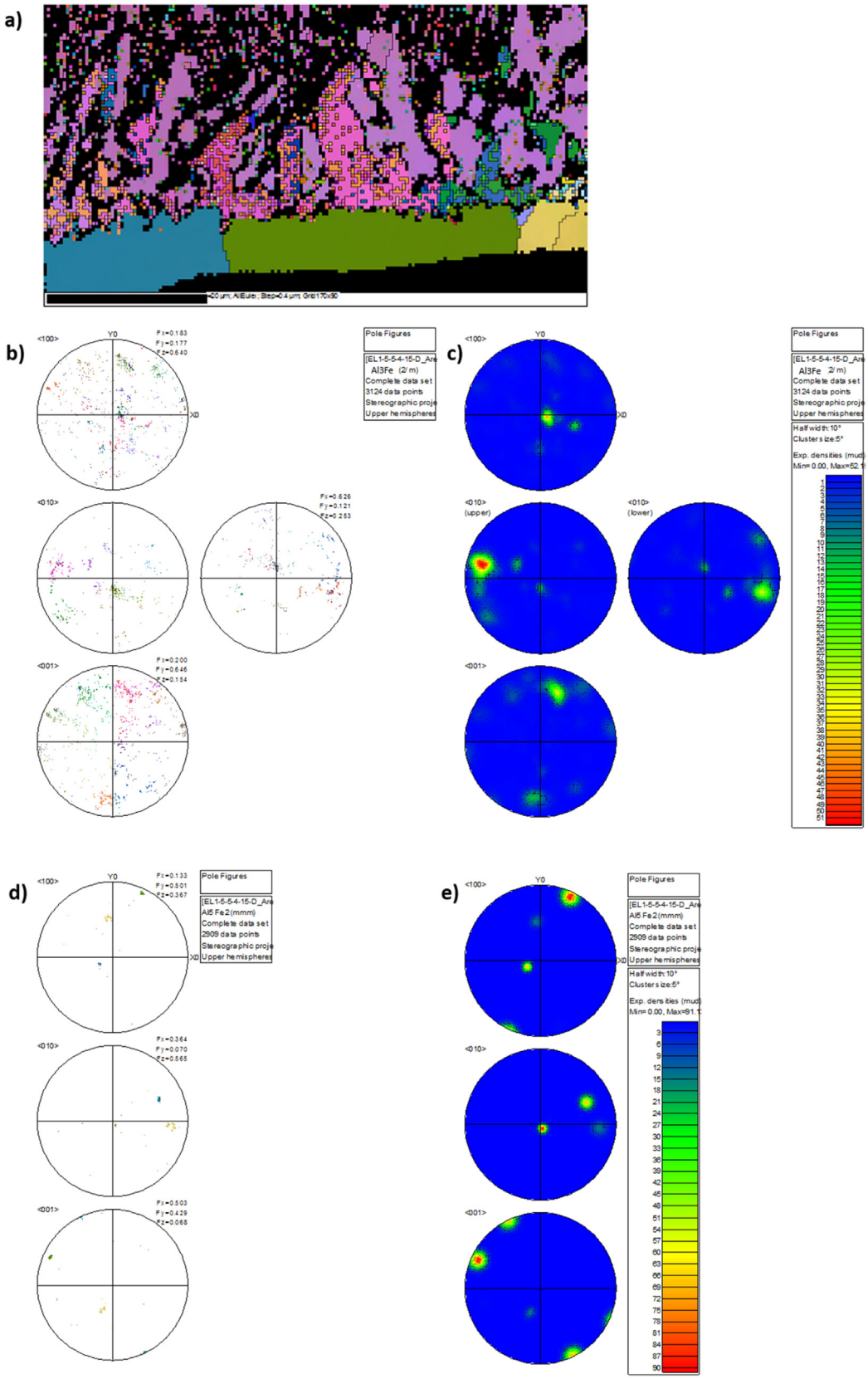

Fig. 14. Crystallographic orientations of grains of a thick intermetallic layer, for the needles (b) and for the main layer (d). Specific orientations of grains could be identified when the density, represented by the coloured scale, respectively for the needles (c) and for the main layer (e), is high (in red). (For interpretation of the references to colour in this figure legend, the reader is referred to the web version of this article.)

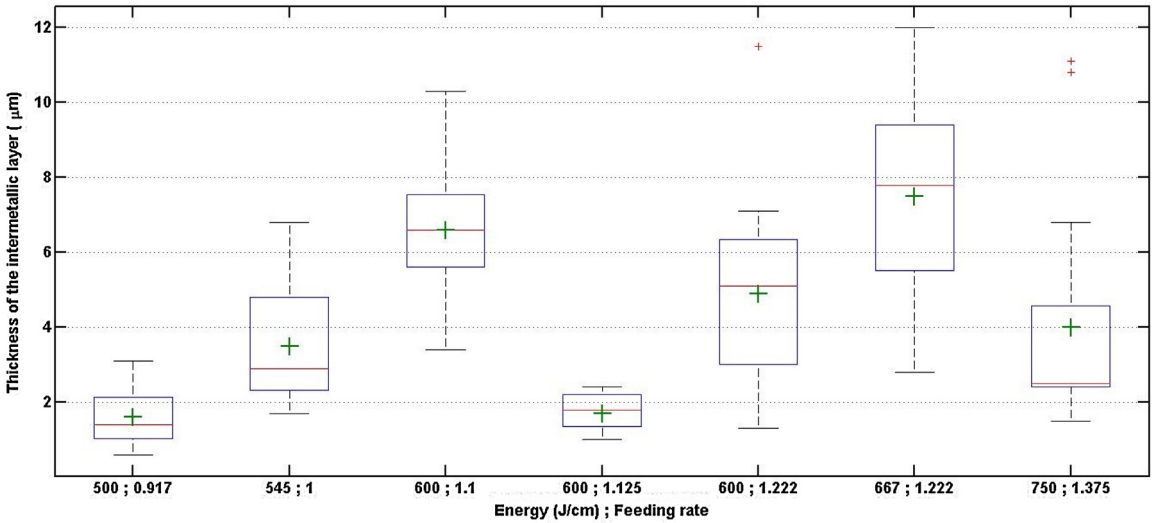

Fig. 15. Maximum thickness of the intermetallic layer (µm) for several energy (J/cm) and feeding rate. For each configuration the green crosses are the average, the red lines are the median, the edges of the boxes are the 25th and 75th percentiles and the dotted lines represent the extreme values of the measurements. (For interpretation of the references to colour in this figure legend, the reader is referred to the web version of this article.)

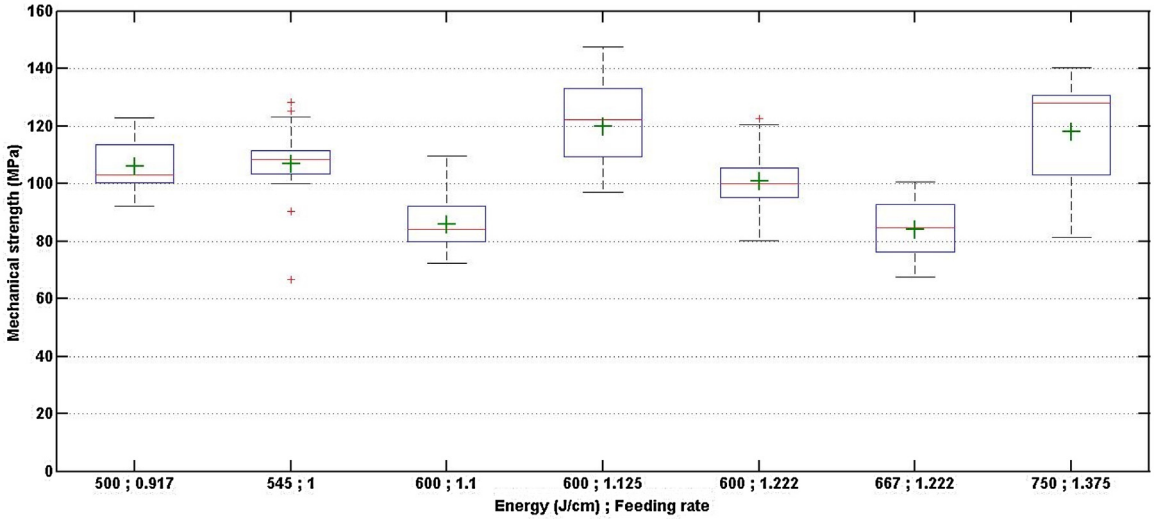

Fig. 16. Averaged mechanical strength (MPa) for several energy (J/cm) and feeding rate. For each configuration the green crosses are the average, the red lines are the median, the edges of the boxes are the 25th and 75th percentiles and the dotted lines represent the extreme values of the measurements. (For interpretation of the references to colour in this figure legend, the reader is referred to the web version of this article.)

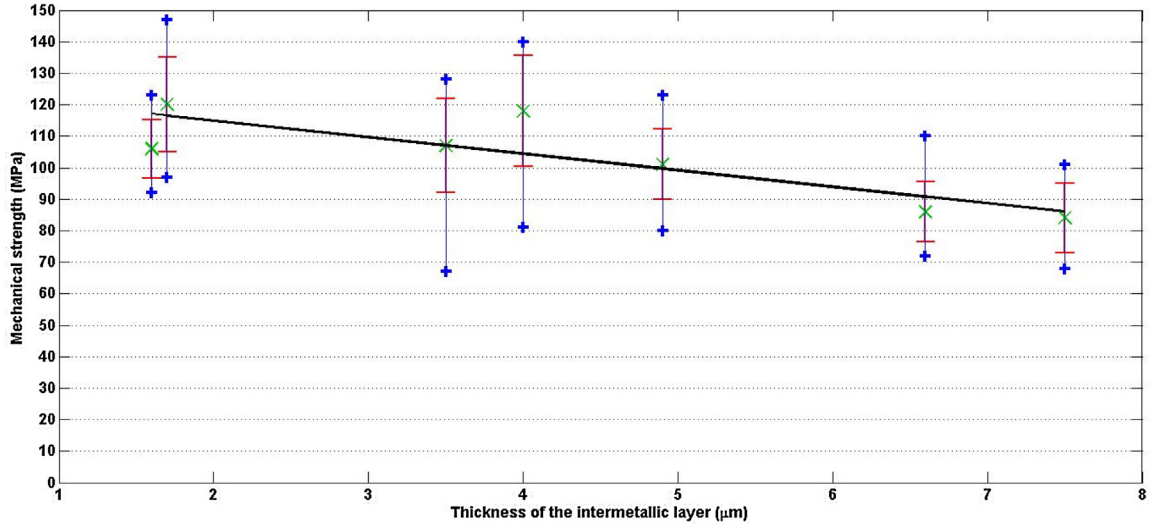

Fig. 17. Averaged values of the maximum thickness of the intermetallic layer (μm) and their corresponding mechanical strength measurements (MPa), green crosses represents averaged values, red lines displays standard deviation and blue crosses minimal and maximal values. The black stretch is the linear interpolation of the measurements with regression coefficient R = −0.84. (For interpretation of the references to colour in this figure legend, the reader is referred to the web version of this article.)

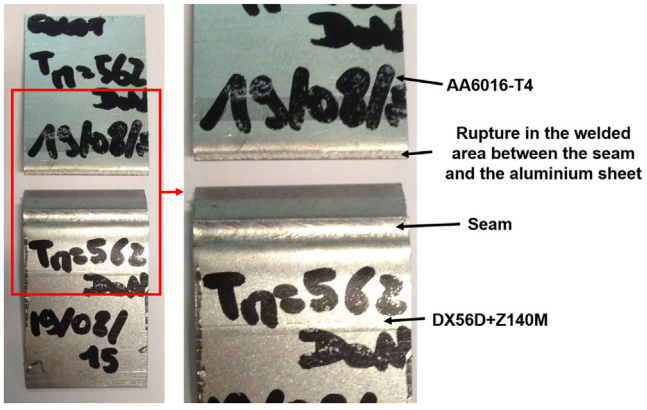

Fig. 18. Rupture in the welded area, between the seam and the aluminium sheet.

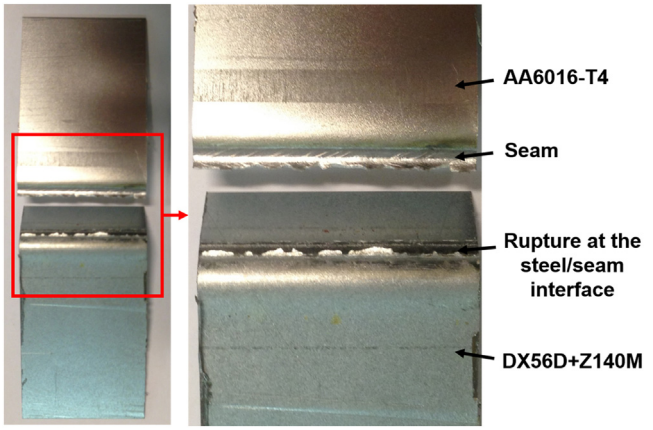

Fig. 19. Rupture at the seam/steel interface where the intermetallic layer is located.

(2) Similarly to the configuration at low brazing speed, joints with thin intermetallic layer and high mechanical strength can be achieved at high brazing speed with no uses of flux.
(3) Involved thermal energy and feed rate of brazing process are valuables variables for optimising intermetallic layer thickness and mechanical strength.
(4) Joints with averaged mechanical strength of 101% of the properties of the filler metal and averaged intermetallic layer of 1.6 μm can be achieved in industrial conditions with an energy of 600 J/cm and a feeding rate of 1.125.

Acknowledgements

The authors acknowledge RENAULT S.A.S. and Arts et Métiers ParisTech for funding this research.

References

[1] Bouché K, Barbier F, Coulet A. Intermetallic compound layer growth between solid iron and molten aluminium. Mater Sci Eng A 1998;249:167–75.
[2] Yeremenko VN, Natanzon YV, Dybkov VI. The effect of dissolution on the growth of the Fe_2Al_5 interlayer in the solid iron–liquid aluminium system. J Mater Sci 1981;16:1748–56.
[3] Chacrone A. Etude métallographique et cinétique de la formation de la couche d'alliage lors des revêtements d'aciers par l'aluminium et l'aluminium-silicium. Thesis. Université de Metz; 1986.
[4] Bruckner J. Considering thermal processes for dissimilar metals—joining steel to aluminium in heat-intensive applications. Fabricator 2003. http://www.thefabricator.com/Metallurgy/Metallurgy_Article.cfm?ID=676. [Accessed 30 September 2016].
[5] Haidara F, Record M-C, Duployer B, Mangelinck D. Phase formation in Al–Fe thin film systems. Intermetallics 2012;23:143–7.
[6] Jia L, Shichun J, Yan S, Cong N, Junke C, Genzhe H. Effects of zinc on the laser welding of an aluminum alloy and galvanized steel. J Mater Process Technol 2015;224:49–59.
[7] Mathieu A, Rajashekhara S, Deschamps A, Cicala E. Dissimilar material joining using laser (aluminium to steel using zinc-based filler wire). Opt Laser Technol 2007;39:652–61.
[8] Pena R. Etudier la possibilité de réalisation d'un assemblage hétérogène acier/aluminium, de bonne qualité et performance mécanique, en utilisant un faisceau laser Nd: YAG. Thesis. école centrale de Lyon; 2005.
[9] Lin J, Ma N, Lei Y, Murakawa H. Shear strength of CMT brazed lap joints between aluminum and zinc-coated steel. J Mater Process Technol 2013;213:1303–10.
[10] Cao R, Gang Y, Chen JH, Wang PC. Cold metal transfer joining aluminium alloys-to-galvanized mild steel. J Mater Process Technol 2013;213:1753–63.
[11] Zhang HT, Feng JC, He P, Zhang BB, Chen JM, Wang L. The arc characteristics and metal transfer behaviour of cold metal transfer and its use in joining aluminium to zinc-coated steel. Mater Sci Eng A 2009;499:111–3.
[12] Su Y, Hua X, Wu Y. Influence of alloy elements on microstructures and mechanical property of aluminum–steel lap joint made by gas metal arc welding. J Mater Process Technol 2014;214:750–5.
[13] Yagati KP, Bathe RN, Rajulapati KV, Bhanu Sankara Rao K, Padmanabham G. Fluxless arc weld-brazing of aluminium alloy to steel. J Mater Process Technol 2014;214:2949–59.
[14] Zhang MJ, Chen GY, Zhang Y, Wu KR. Research on microstructure and mechanical properties of laser keyhole welding-brazing of automotive galvanized steel to aluminium alloy. Mater Des 2013;45:24–30.
[15] Dharmendra C, Rao KP, Wilden J, Reich S. Study on laser welding-brazing of zinc coated steel to aluminum alloy with a zinc based filler. Mater Sci Eng A 2011;528:1497–503.
[16] Potesser M, Schoeberl T, Antrekowitsch H, Bruckner J. In: Howard SM, Stephens RL, Newman CJ, Hwang J-YJ, Gokhale AM, Chen TT, editors. The characterization of the intermetallic Fe–Al layer of steel–aluminum welding, EPD Congress 2006. The Minerals, Metals & Materials Society; 2006.
[17] Frank S. Flux-free laser joining of aluminium and galvanized steel. J Mater Process Technol 2015;222:365–72.
[18] Koltsov A, Bailly N, Cretteur L. Wetting and laser brazing of Zn-coated steel products by Cu–Si filler metal. J Mater Sci 2010;45:2118–25.
[19] Lehto P, Remes H, Saukkonen T, Hanninen H, Romanoff J. Influence of grain size distribution on the Hall–Petch relationship of welded structural steel. Mater Sci Eng A 2014;592:28–39.
[20] Quek SS, Chooi ZH, Wu Z, Zhang YW, Srolovitz DJ. The inverse Hall–Petch relation in nanocrystalline metals: a discrete dislocation dynamics analysis. J Mech Phys Solids 2016;88:252–66.
[21] Vrenken J, Goos C, Van der Veldt T, Braunschweig W. Fluxless laser brazing of aluminium to steel. Joining Automot Eng 2009.

Guillaume Filliard is a PhD Student at the Mechanics, Surfaces and Materials Processing (MSMP) laboratory of the French engineering school Arts et Métiers ParisTech (ENSAM) in collaboration with the international car manufacturer RENAULT working on joining steel and aluminium at high speed for specific automotive application, he graduated as an engineer at Arts et Métiers ParisTech in 2013.

Mohamed El Mansori is a Professor in the Department of Mechanical, Material Science and Manufacturing Engineering at the Arts et Métiers ParisTech (ENSAM). He also served as Deputy General Director in Charge of Research & Innovation of Arts et Métiers ParisTech and chaired the Mechanical Engineering and Manufacturing Research Group (LMPF Laboratory), France. He received his BSc in Physics from the University of Hassan II in 1993 (Casablanca, Morocco), and his PhD in Mechanical Engineering from the Institut National Polytechnique de Lorraine (INPL) in 1997 at Nancy, France.

Lucio Tirado is a laser specialist at the car manufacturer RENAULT researching and developing industrial laser joining applications at Renault for 15 years. In particular, he worked on the development and the industrial implantation of steel brazing process for roof/body-side joining and is looking on new heterogeneous joining process for car weight reduction.

Sabeur Mezghani is a Master of Conference at the Arts et Métiers ParisTech (ENSAM), he received is PhD in Mechanical and Civil Engineering from the Ecole Centrale de Lyon (ECL) engineering school in 2005.

Christian Bremont is a brazing and welding process Expert at RENAULT and engineer of the Institut National des Sciences Appliquées (INSA).

Mathieu De Metz-Noblat is the Head of the Innovations and Assembly research and development team of RENAULT. He graduated as an engineer of the Ecole Catholique des Arts et Métiers de Lyon (ECAM) in 1998.